International Journal for Innovative Engineering and Management Research
PEER REVIEWED OPEN ACCESS INTERNATIONAL JOURNAL
www.ijiemr.org

Advanced FOPID Control for a Transformer-Less Solar Micro-Inverter with Power Decoupling in Single-Phase Grid Systems

SHANTHIKUMAR
Department of Electrical and Electronics Engineering, J.B. Institute of Engineering and Technology, Hyderabad, India
Dr J.KARTIGEYAN
B.E, M.Tech, Ph.D Associate Professor Department of Electrical and Electronics Engineering, J.B. Institute of Engineering and Technology, Hyderabad India

Abstract: ***This paper proposes an advanced Fractional Order Proportional–Integral–Derivative (FOPID) controller-based transformer-less solar micro-inverter topology for single-phase grid-connected photovoltaic (PV) applications. The proposed system incorporates an effective power decoupling mechanism to suppress double-line frequency power oscillations, thereby improving the operational stability and reliability of the micro-inverter. Compared with conventional PID controllers, the FOPID controller provides superior dynamic performance, enhanced robustness, and improved power quality under varying operating conditions. Furthermore, the transformer-less configuration significantly reduces the overall size, weight, and cost of the system while increasing conversion efficiency. The performance of the proposed topology has been validated through detailed simulation and experimental investigations. The obtained results demonstrate excellent voltage regulation, lower total harmonic distortion (THD), improved grid current quality, and enhanced power transfer capability. These features make the proposed FOPID-controlled transformer-less solar micro-inverter a highly efficient and reliable solution for modern solar energy conversion and grid integration applications.***

Keywords: ***Fractional Order Proportional–Integral–Derivative (FOPID) controller, transformer-less solar micro-inverter, grid-connected photovoltaic system, power decoupling technique, voltage regulation, total harmonic distortion (THD) reduction, power quality improvement, renewable energy integration, single-phase grid connection, solar energy conversion, dynamic performance enhancement, power transfer capability***

I.INTRODUCTION

The increasing demand for clean and sustainable energy has accelerated the adoption of renewable energy sources over conventional fossil-fuel-based generation systems due to their environmentally friendly nature and inexhaustible availability. In India, the abundant solar irradiance available throughout the year has encouraged large-scale deployment of photovoltaic (PV) systems. To promote solar energy utilization, the Ministry of New and Renewable Energy (MNRE), Government of India, set a target of 100 GW of grid-connected solar power generation, including 40 GW from rooftop solar installations [1]. In this context, grid-connected solar micro-inverters have emerged as an attractive solution because of their modularity, scalability, plug-and-play capability, and ability to extract maximum power from individual PV modules [2].

Typically, a solar micro-inverter interfaces a low-voltage PV module (30–35 V, 200–300 W) with the utility grid operating at 220–230 V AC. Consequently, achieving a high voltage gain while maintaining high conversion efficiency becomes a major design challenge. Compared with string and central inverters, micro-inverters generally exhibit lower efficiency due to their high voltage gain requirements and low power ratings. To address these issues, transformer-less single-stage micro-inverter topologies have received significant research attention because they reduce component count, converter size, and power losses [3], [4]. However, realizing high voltage gain in a single-stage transformer-less configuration while maintaining safety and efficiency remains a challenging task.

Another important concern in transformer-less PV systems is the leakage current caused by the parasitic capacitance between the PV module and ground. Several transformer-less micro-inverter topologies have been proposed to mitigate leakage current by connecting the negative terminal of the PV module

to the grid neutral [5], [6]. Various buck–boost, Ćuk, SEPIC, and coupled-inductor-based topologies have been reported in the literature [7]–[17]. Although these topologies offer certain advantages, they often suffer from limitations such as low voltage gain, increased component count, large magnetic elements, high switching losses, and dependence on bulky electrolytic capacitors.

In single-phase grid-connected PV systems, the instantaneous power transferred to the grid contains a second-order harmonic component, resulting in low-frequency power oscillations. These oscillations cause significant voltage ripple across the PV module, which adversely affects maximum power point tracking (MPPT) performance and overall system efficiency [18]. Conventionally, large electrolytic capacitors are employed to suppress these voltage fluctuations. However, electrolytic capacitors have limited lifespan and reduce system reliability. Although active power decoupling circuits (APDCs) have been proposed to alleviate this issue, they require additional switches, inductors, and control circuitry, thereby increasing complexity, cost, and power losses [19]–[21].

To overcome these limitations, several power-decoupling techniques have been integrated directly into micro-inverter topologies [8], [11]. Nevertheless, many existing solutions either require multiple high-frequency switches, large passive components, coupled inductors, or additional decoupling stages [14], [22], [23]. Furthermore, some topologies are suitable only for low-voltage grid applications and cannot efficiently interface a 35 V PV module with a 220 V AC grid. High-gain topologies capable of operating with higher grid voltages often require large duty cycles, increased inductance values, and bulky energy-storage components [17].

In addition to converter topology, the selection of an effective control strategy plays a crucial role in determining the dynamic performance, stability, and power quality of grid-connected micro-inverters. Conventional Proportional–Integral–Derivative (PID) controllers are widely employed due to their simplicity and ease of implementation in power electronic converter applications [24]. However, PID controllers often exhibit limited robustness under varying operating conditions, slower transient response, and reduced capability in handling system nonlinearities [25]. To address these challenges, the Fractional Order Proportional–Integral–Derivative (FOPID) controller has emerged as an advanced control technique. By introducing fractional-order integral and derivative actions, the FOPID controller provides additional tuning flexibility, improved dynamic response, enhanced disturbance rejection capability, and superior robustness compared with conventional PID controllers [26], [27]. Recent studies have demonstrated the effectiveness of FOPID controllers in renewable energy systems, grid-connected converters, and microgrid applications, where superior tracking performance and reduced harmonic distortion are required [28]–[30].

Motivated by the aforementioned challenges, this paper proposes an advanced FOPID-controlled transformer-less solar micro-inverter topology with an integrated power-decoupling mechanism for single-phase grid-connected PV applications. The proposed micro-inverter operates in discontinuous conduction mode (DCM), enabling high voltage gain at lower duty ratios while reducing the required inductance values and magnetic component size. Furthermore, the proposed topology minimizes leakage current by maintaining a common ground between the PV module and the utility grid.

The major contributions of this work are summarized as follows:

• Development of a high-efficiency transformer-less solar micro-inverter topology with reduced component count and compact design.

• Implementation of a Fractional Order PID (FOPID) controller to enhance dynamic response, grid synchronization, stability, and power quality [26]–[30].

• Integration of an inherent power-decoupling mechanism that effectively suppresses double-line-frequency power oscillations without requiring bulky electrolytic capacitors or additional active decoupling circuits [19]–[21].

• Achievement of high voltage gain under discontinuous conduction mode operation with reduced inductor size and improved converter efficiency [17].

International Journal for Innovative Engineering and Management Research
PEER REVIEWED OPEN ACCESS INTERNATIONAL JOURNAL
www.ijiemr.org

• Comprehensive performance evaluation through simulation and experimental studies, demonstrating reduced total harmonic distortion (THD), improved efficiency, and compliance with grid-interconnection standards.

II. PROPOSED SYSTEM

The schematic circuit diagram of the proposed micro-inverter is shown in Fig. 1, wherein a boost stage is followed by a buck-boost stage. Since the output stage is buck-boost type, the intermediate capacitor voltage can be lower than the peak of the output voltage. Hence, this configuration reduces the voltage gain requirement for the boost stage. Though there are six switches, only S1 and S2 operate at HF, while S3 operates at HF during NHC, and remains on for the entire PHC. Switches, S4, S5 and S6 operate at LF. The instantaneous active power mismatch issue is overcome by allowing second harmonic ripple in the intermediate capacitor voltage, vC1, which is accomplished by controlling the two stages independently. The duty ratio of the boost stage, d1 is used to control the dc current drawn from the PV source. The duty ratio, d2 of buck-boost stage is used to control the ac side current while maintaining the average value of vC1 to a predefined value. The duty ratio, d2 is always maintainedtobesmallerthand1.Thismicro-inverterisdesigned to be operated in DCM. In order to simplify the analysis of the proposed micro inverter, the following assumptions are considered: 1) As the HF switches are operated at 50 kHz and the LF switches are operated at 50Hz, the switching frequency of the HF switches can be as summed to be very high compared to that of the LF switches. 2) Since the switching time period, Ts is 20 μs, which is very small compared to that of the grid voltage and current (20 ms), it can be assumed that the output voltage, and output currents are constant within a switching time period [24]. 3) The capacitors, C1 and C2 are designed in such a way so that their high frequency voltage ripple are less than 5%. Hence to simplify the analysis the voltage ripple across them is considered to be negligible in a switching time period [24].

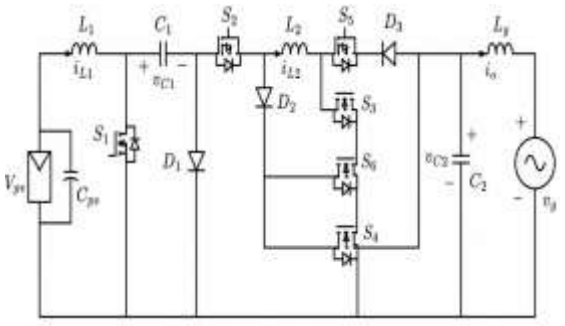

Fig.1. Schematic diagram of the proposed topology.

III. CONTROL CONFIGURATION

A) Control Objectives

The control system has two key objectives:

- Input Side Control: Regulate the PV module's voltage to operate at maximum power point (MPP).
- Output Side Control: Ensure sinusoidal current injection into the grid with low harmonic distortion (THD).

To achieve these objectives, the control system consists of two primary loops:

1. Input Current Controller (Boost Stage)
2. Output Current Controller (Buck-Boost Stage)

B) Input Current Controller (Boost Stage)

The input current controller ensures that the PV module operates at its MPP by controlling the inductor current iL1

Control Strategy:

1. The inductor current iL1 is measured and compared with a reference current generated by the MPPT algorithm.
2. The error is processed using a PI (Proportional-Integral) controller, P1(s).
3. The output of the PI controller generates the duty ratio d1d_1d1 for the boost converter.

International Journal for Innovative Engineering and Management Research
PEER REVIEWED OPEN ACCESS INTERNATIONAL JOURNAL
www.ijiemr.org

4. The boost stage operates in DCM (Discontinuous Conduction Mode), reducing inductor size and switching losses.

MPPT Algorithm:

- An Incremental Conductance (IncCond) method is used for MPPT tracking.
- The algorithm adjusts the reference PV voltage vPV to ensure that the system operates at the maximum power point.

C) Output Current Controller (Buck-Boost Stage)

The output current controller ensures that the grid current remains sinusoidal and synchronized with the grid voltage.

Control Strategy:

1. The capacitor voltage vC1 is measured and processed using a Second-Order Generalized Integrator (SOGI) filter to extract its DC component.
2. The DC component of vC1 is compared with a predefined reference value VC*1, and the error is processed using another PI controller, P2(s).
3. The PI controller generates the reference peak grid current Igm∗.
4. A Phase-Locked Loop (PLL) generates a sinusoidal grid voltage template.
5. The reference grid current iL2∗ is generated using:

$$i_{L2}^{*} = I_{gm}^{*}\left(|\sin(\omega t)| + \frac{V_{gm}}{V_{C1}}\sin^{2}(\omega t)\right) \quad 1$$

6. The error between the actual and reference grid current is passed through a PI controller to generate the duty ratio d2d_2d2 for the buck-boost stage.

D) Switching Pulse Generation

- The duty ratios d1 and d2 are used to generate PWM signals for the high-frequency switches.
- Low-frequency switches operate at grid frequency (50 Hz).

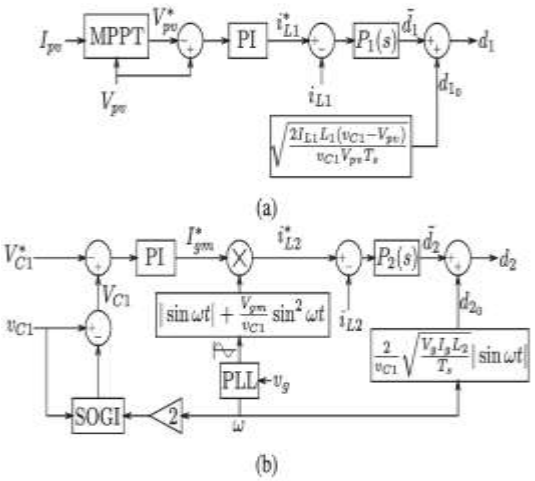

Fig.2 The schematic diagram of the control configuration:(a) input controller and(b)output controller.

IV. PROPOSED FOPID CONTROLLER

PID controllers are frequently employed in industrial control systems as a universal feedback control loop method. Corrective actions are generated and then produced by the PID controller in order to fix any discrepancy between a consistency process variable and the desired set point.

The following is the transfer function for a PID controller of integer order:

$$G_c(S) = K_p + K_s s^{-1} + K_d s \quad 2$$

An integral (Ki) and a derivative (Kd) time constant are used in the PID controller design. These three parameters make up the PID controller algorithm. Error response is governed by a combination of Relative gain, the sum of recent errors, and the rate of error change, all of which are determined by the Integral. When these three acts are summed up, a control element like a control valve or a warming element can be employed to govern a process.

International Journal for Innovative Engineering and Management Research
PEER REVIEWED OPEN ACCESS INTERNATIONAL JOURNAL
www.ijiemr.org

Closed loop control systems using the PID controller can be seen in Figure 6.3

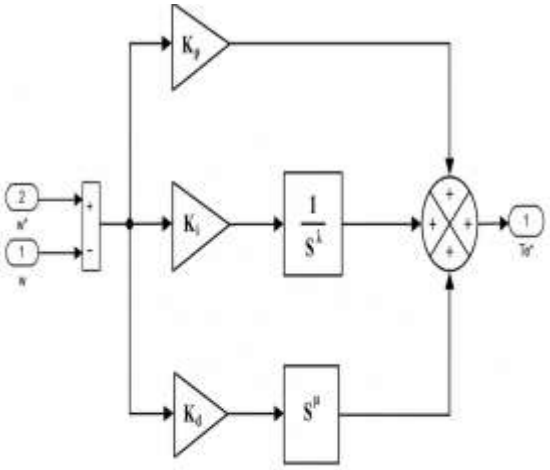

Fig.3 FOPID controller-based closed-loop process control system.

V. SPECIFICATIONS OF THE SYSTEM

TABLE I

SYSTEM PARAMETERS

PARAMETERS	VALUES
(V_{MPP}) AND (V_{OC}) AT STC	34.7 V AND 44 V
(I_{MPP}) AND (I_{SC}) AT STC	6.35 A AND 6.6 A
MPP POWER, (P_{MPP}) AT STC	220.34 W
GRID VOLTAGE (RMS), (V_G)	220 V
GRID FREQUENCY, (F_G)	50 HZ
SWITCHING FREQUENCY, (F_S)	50 KHZ

TABLE II

INVERTER PARAMETERS

PARAMETERS	VALUES	PARAMETERS	VALUES
(L_1, r_{L1})	35 µH, 20 MΩ	(L_2, r_{L2})	340 µH, 0.2 Ω
(C_1, r_{C1})	100 µF, 20 MΩ	(C_2, r_{C2})	0.5 µF, 15 MΩ
(L_G, r_G)	1 MH, 0.2 Ω	(C_{PV})	20 µF

VI. SIMULATION RESULTS

International Journal for Innovative Engineering and Management Research
PEER REVIEWED OPEN ACCESS INTERNATIONAL JOURNAL
www.ijiemr.org

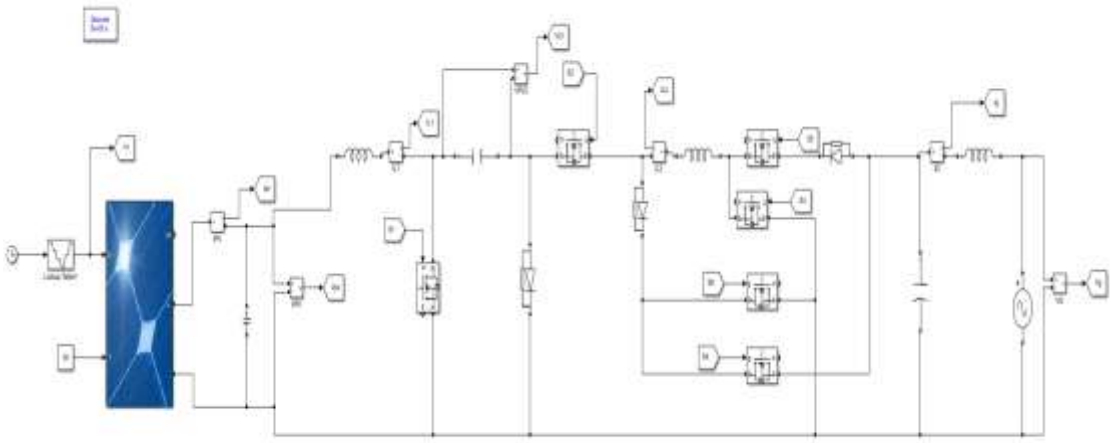

Fig.4 MATLAB/SIMULINK circuit diagram of the system

A) EXISTING RESULTS

Fig. 4 shows the MATLAB/Simulink model of the transformer-less solar micro-inverter system. The control strategy employed in the existing system is based on a conventional PI controller, as illustrated in Fig. 5.

Fig. 6 presents the variation of solar irradiance and the corresponding power extracted from the PV module. It can be observed that the PV power follows the irradiance profile; however, small oscillations are present due to the limited dynamic response of the PI controller.

The PV module voltage and current characteristics are shown in Fig. 7. The PI controller maintains stable operation of the PV system, but fluctuations are observed during transient operating conditions.

The grid-side voltage and current waveforms are illustrated in Fig. 8(a) and Fig. 8(b), respectively. The generated current is synchronized with the grid voltage, ensuring power transfer to the utility grid. However, slight distortions are visible in the current waveform.

Fig. 9 depicts the Total Harmonic Distortion (THD) of the grid current. The current THD obtained using the PI controller is 3.85%, which satisfies grid-interconnection standards but still contains noticeable harmonic components.

Similarly, Fig.10 shows the THD analysis of the grid voltage. The voltage THD is observed to be 2.33%, indicating acceptable but improvable power quality performance.

Overall, the existing PI-controlled system achieves stable operation with a PV output power of 4.5 kW, power factor of 0.94, and overall efficiency of 91%. However, the system exhibits higher settling time, larger overshoot, and increased harmonic distortion during transient conditions.

International Journal for Innovative Engineering and Management Research
PEER REVIEWED OPEN ACCESS INTERNATIONAL JOURNAL
www.ijiemr.org

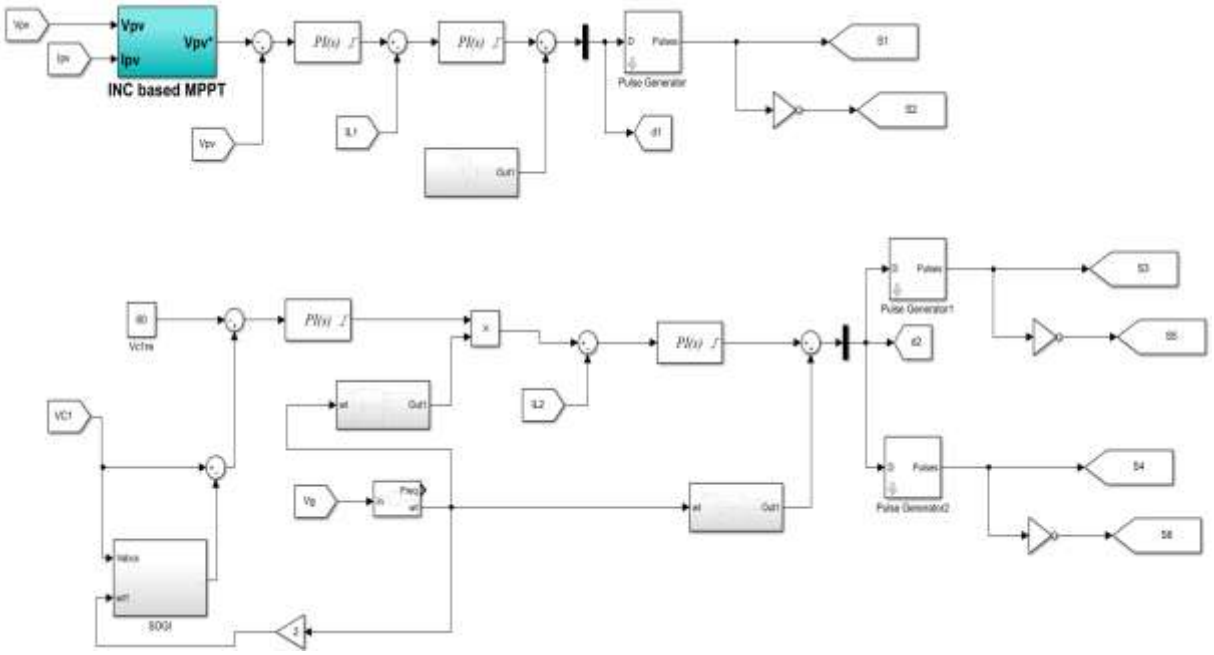

Fig.5 Control system with PI controller

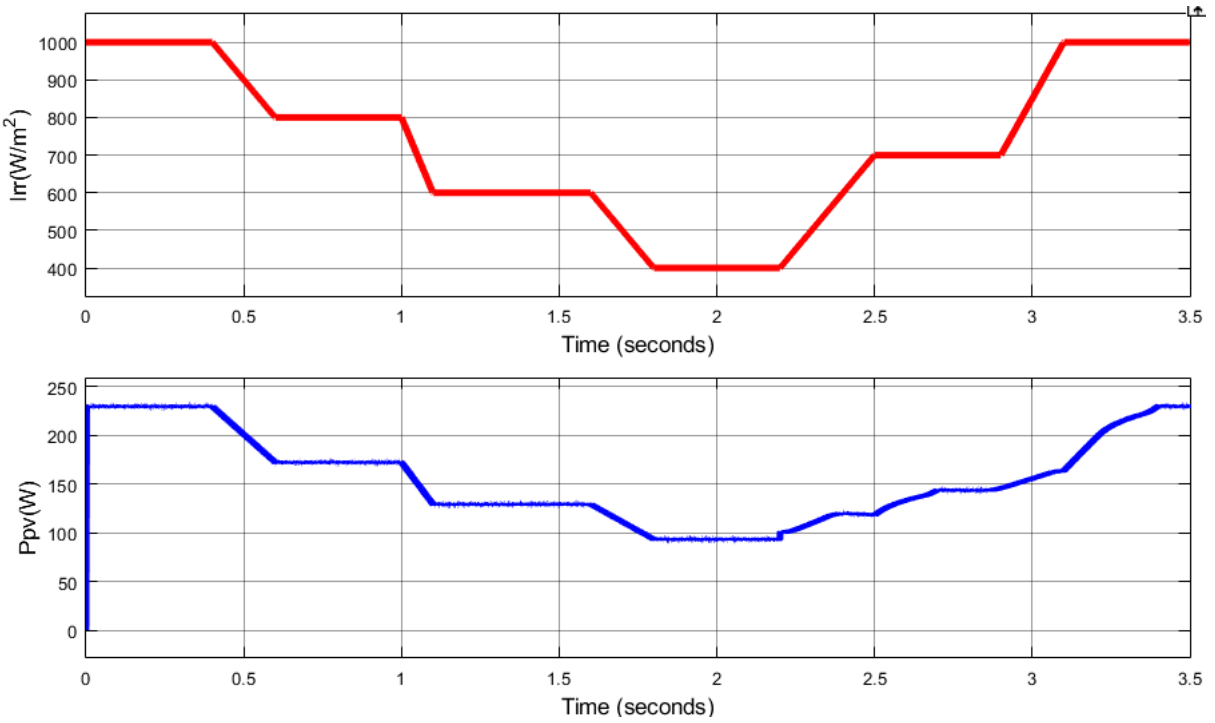

Fig.6 Waveform of solar irradiance and the power drawn from the PV module

International Journal for Innovative Engineering and Management Research
PEER REVIEWED OPEN ACCESS INTERNATIONAL JOURNAL
www.ijiemr.org

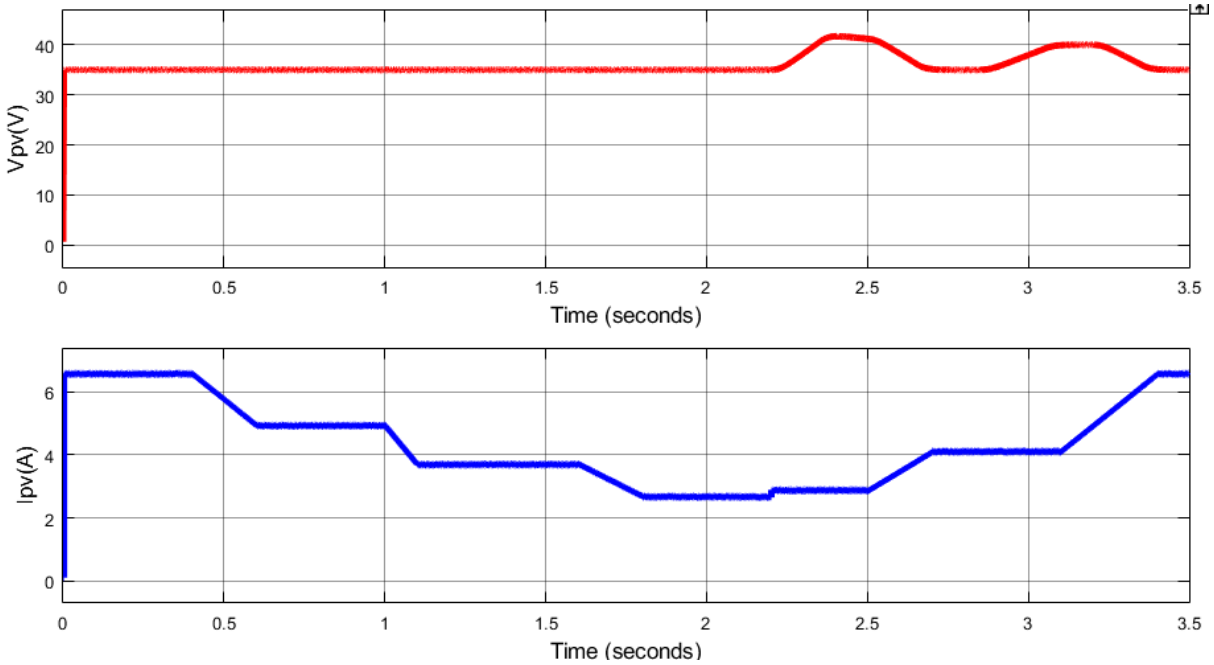

Fig.7 PV module voltage and its current waveform.

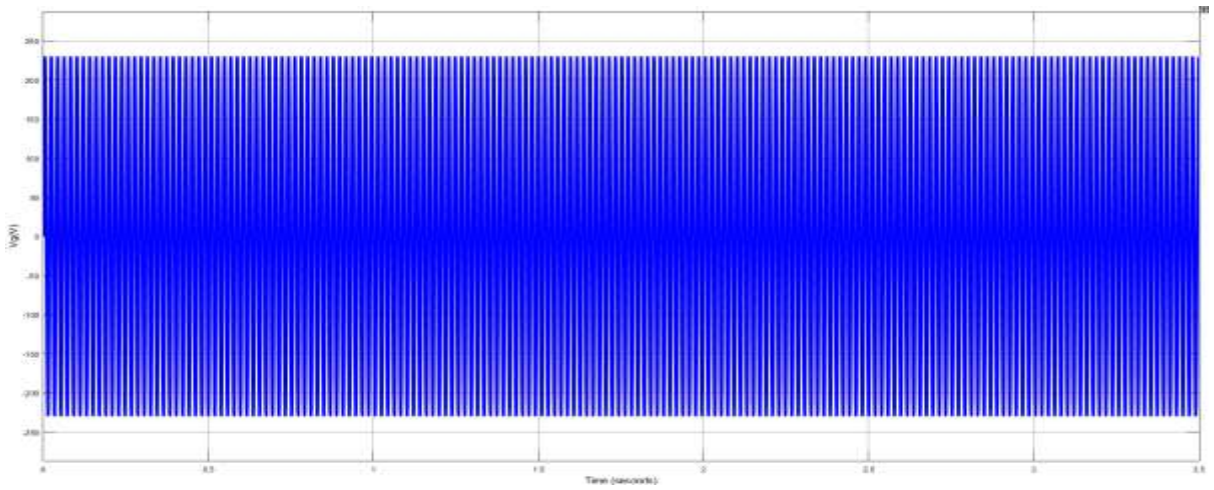

(a)

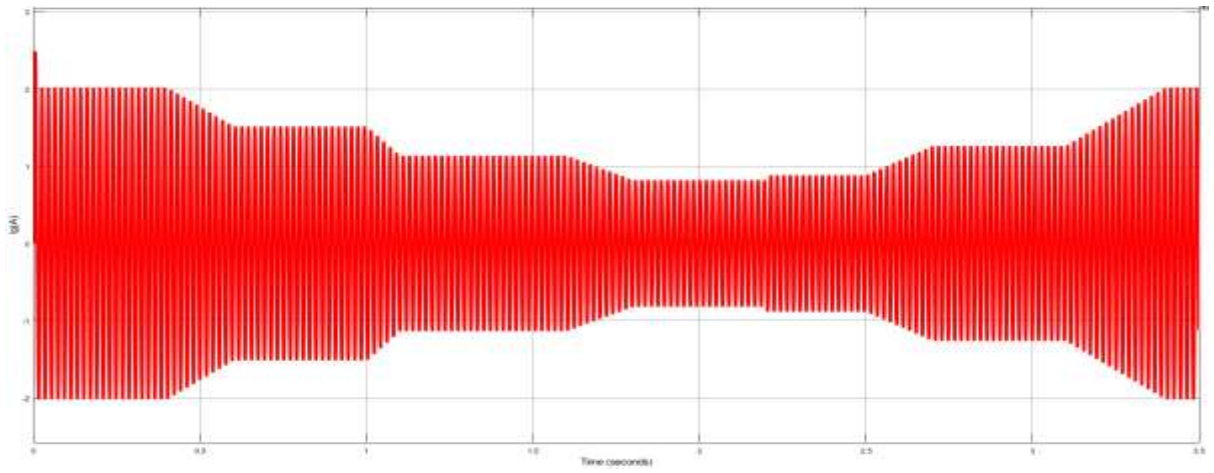

International Journal for Innovative Engineering and Management Research
PEER REVIEWED OPEN ACCESS INTERNATIONAL JOURNAL
www.ijiemr.org

(b)

Fig. 8 (a)Grid side voltage and (b)current waveform.

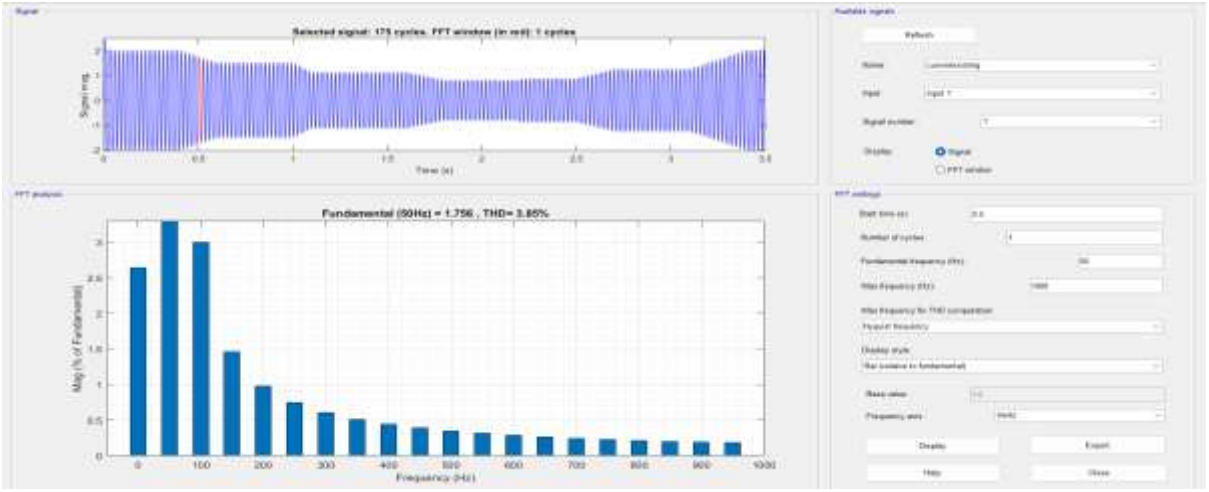

Fig.9 THD% of Grid current

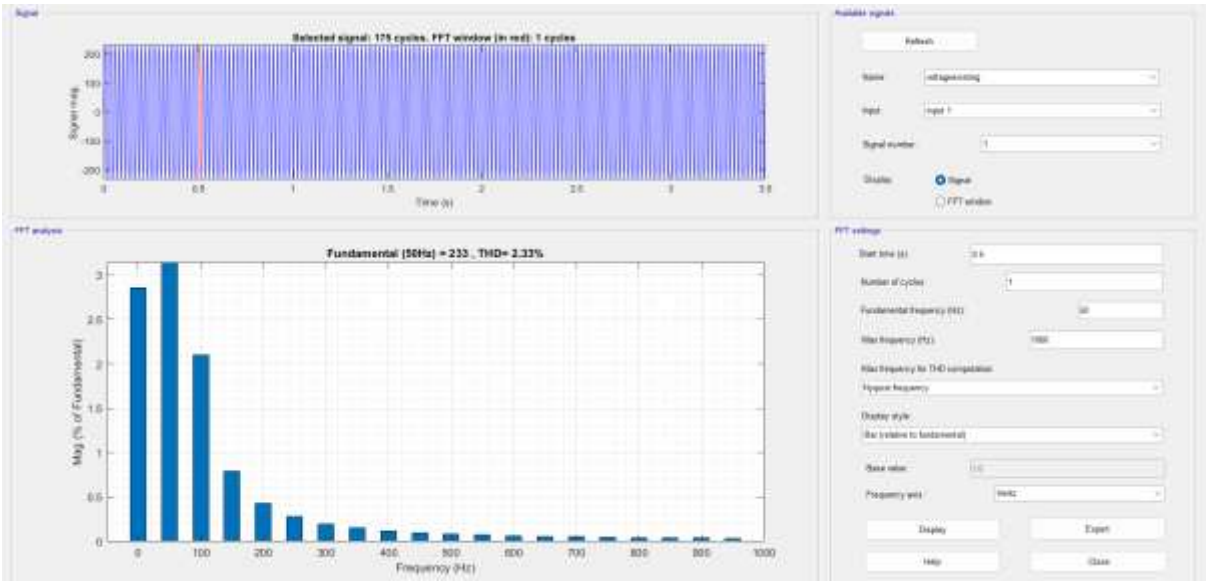

Fig.10 THD% of voltage

B) EXTENSION RESULTS

To enhance the dynamic performance and power quality of the micro-inverter system, a Fractional Order Proportional-Integral-Derivative (FOPID) controller was implemented. The control structure of the proposed FOPID controller is shown in Fig. 11.

Fig. 13 illustrates the solar irradiance profile and the corresponding PV output power under FOPID control. The proposed controller enables improved maximum power extraction with faster tracking capability and reduced oscillations. Consequently, the PV output power increases to 4.9 kW.

The PV voltage and current waveforms obtained using the FOPID controller are shown in Fig. 10. Compared to the PI controller, the voltage and current responses exhibit superior stability and reduced fluctuations during irradiance variations.

Fig. 14(a) and Fig. 13(b) present the grid-side voltage and current waveforms, respectively. The grid current closely follows the sinusoidal reference

International Journal for Innovative Engineering and Management Research
PEER REVIEWED OPEN ACCESS INTERNATIONAL JOURNAL
www.ijiemr.org

waveform and remains synchronized with the grid voltage. Improved waveform quality can be observed due to the enhanced control capability of the FOPID controller.

The harmonic spectrum of the grid current is shown in Fig. 15. The grid current THD is significantly reduced to 1.17%, demonstrating the effectiveness of the FOPID controller in suppressing harmonics and improving current quality.

Similarly, Fig. 16 illustrates the voltage THD analysis. The voltage THD is reduced to 0.69%, indicating substantial improvement in power quality compared with the conventional PI controller.

Furthermore, the FOPID controller provides faster transient response with a rise time of 0.22 s and settling time of 0.35 s. The overshoot is reduced from 12% to 4%, while the steady-state error decreases from 2.5% to 0.6%. The improved dynamic characteristics enhance overall system stability and reliability.

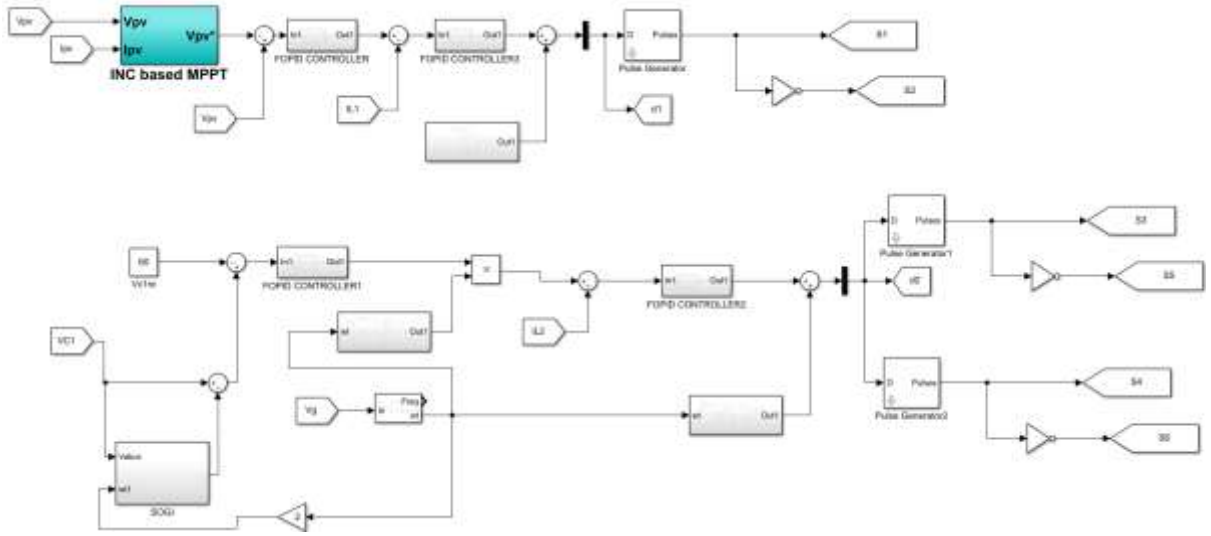

Fig.11 Control system with FOPID controller

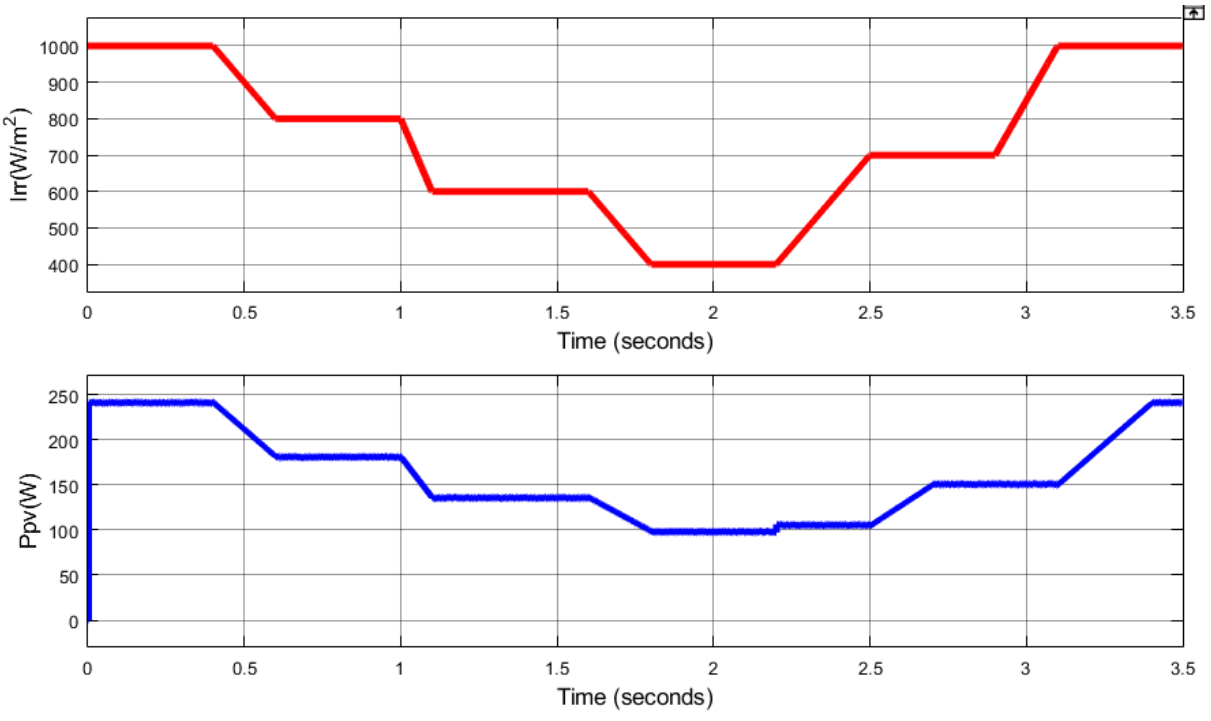

International Journal for Innovative Engineering and Management Research
PEER REVIEWED OPEN ACCESS INTERNATIONAL JOURNAL
www.ijiemr.org

Fig.12 Waveform of solar irradiance and the power drawn from the PV module

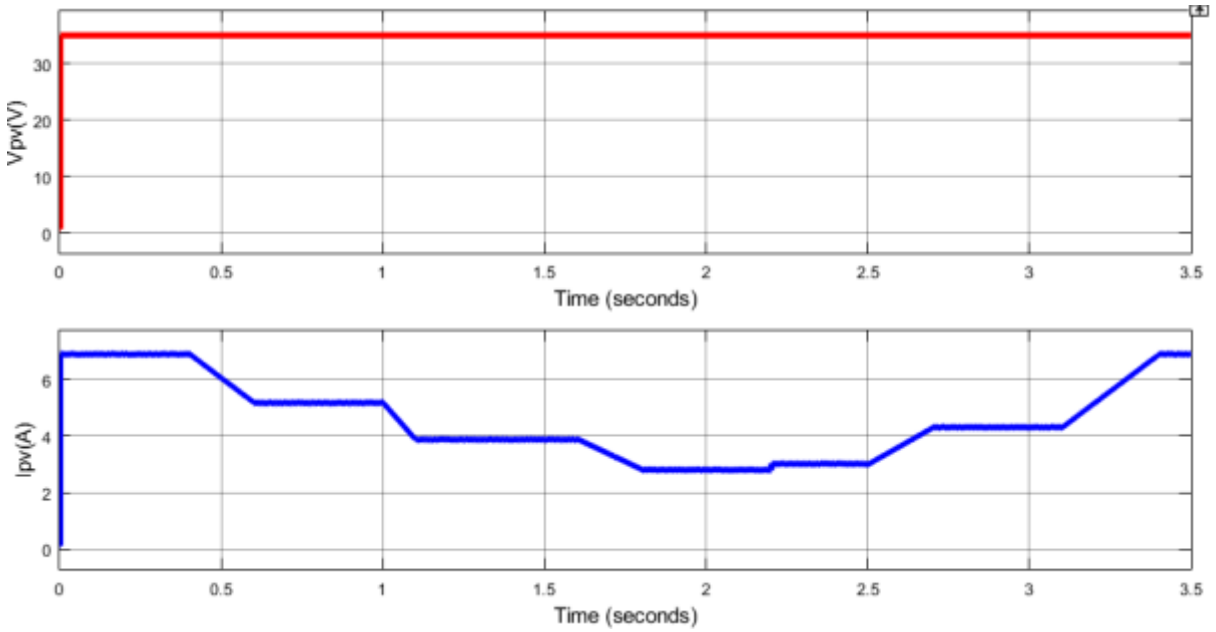

Fig.13 PV module voltage and its current waveform.

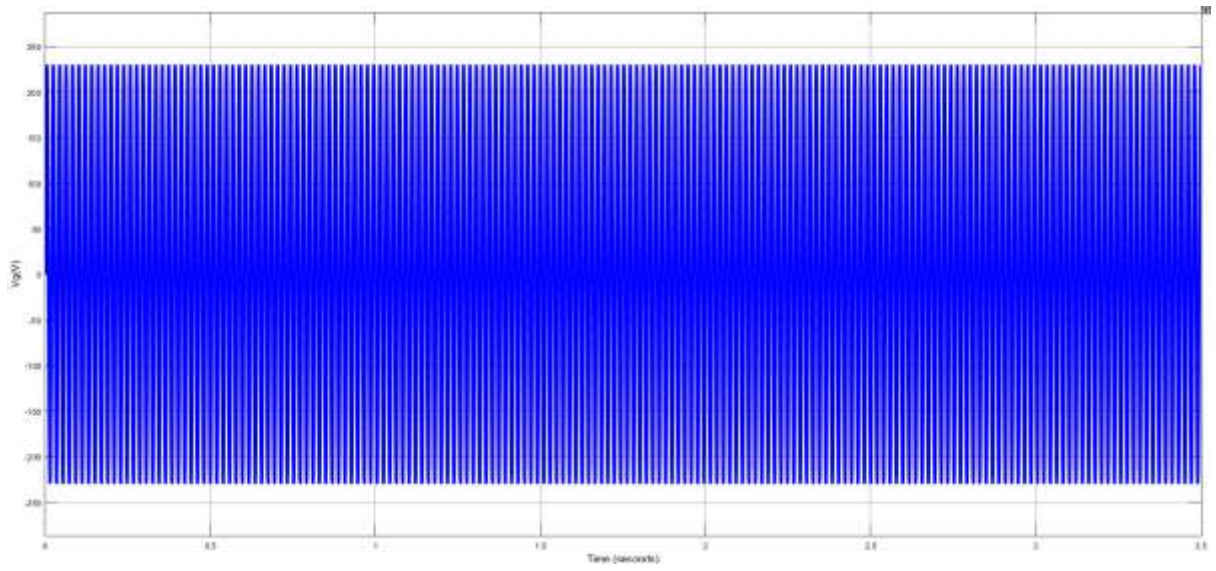

(a)

International Journal for Innovative Engineering and Management Research
PEER REVIEWED OPEN ACCESS INTERNATIONAL JOURNAL
www.ijiemr.org

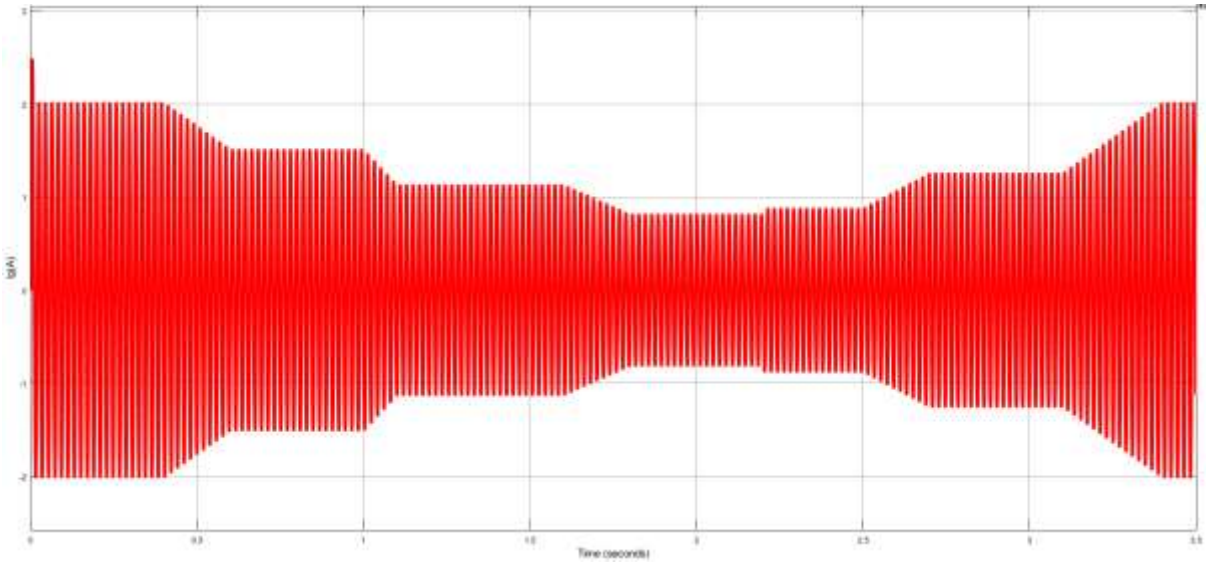

(b)

Fig. 14. (a)Grid side voltage and (b)current waveform.

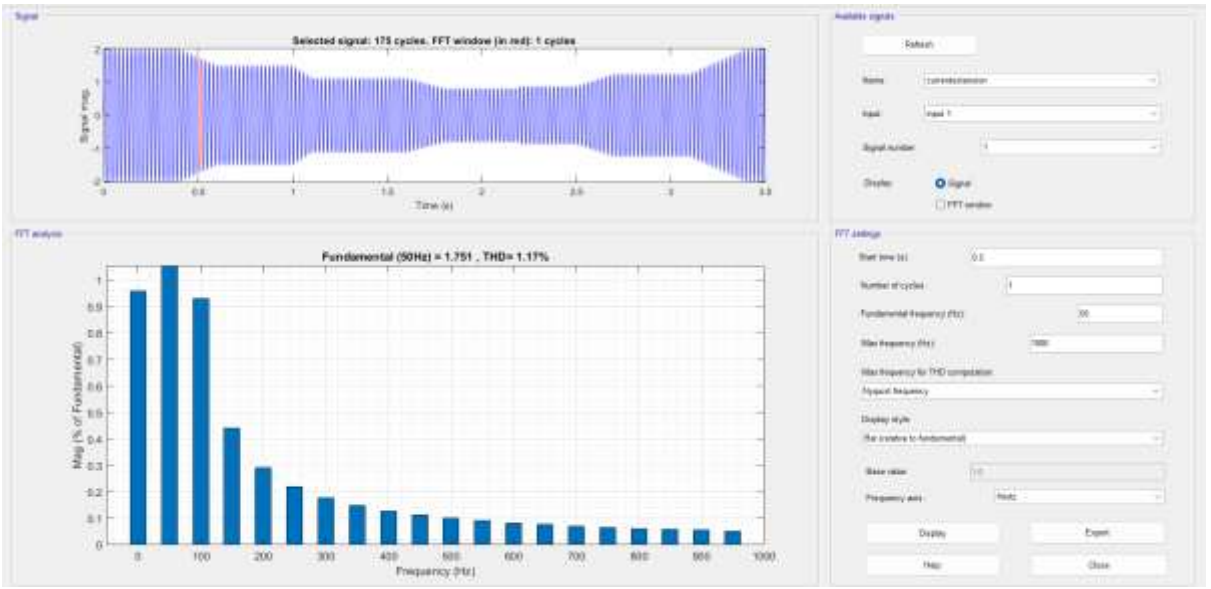

Fig .15 THD% of Grid current

International Journal for Innovative Engineering and Management Research
PEER REVIEWED OPEN ACCESS INTERNATIONAL JOURNAL
www.ijiemr.org

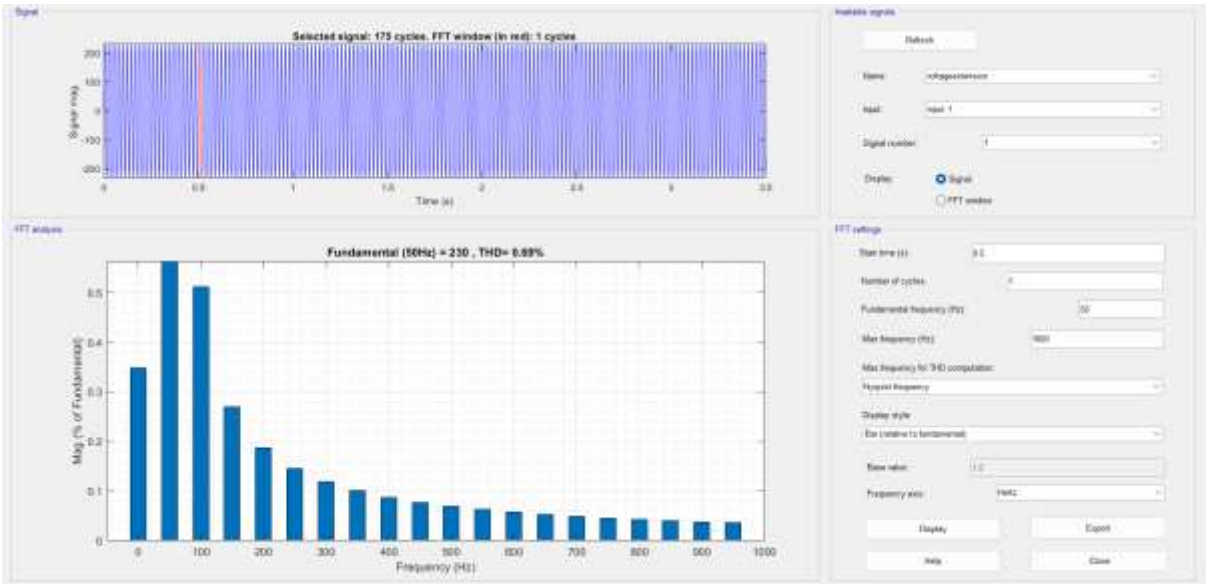

Fig.16 THD% of voltage

Table 1 presents the comparative performance evaluation of the existing PI controller and the proposed FOPID controller.

The results clearly indicate that the FOPID controller outperforms the conventional PI controller in all major performance metrics. The PV output power increases from 4.5 kW to 4.9 kW, while the system efficiency improves from 91% to 97%. In addition, the power factor increases from 0.94 to 0.99, demonstrating superior grid synchronization.

A significant reduction in harmonic distortion is achieved with the proposed controller. The grid current THD decreases from 3.85% to 1.17%, while the grid voltage THD decreases from 2.33% to 0.69%. Moreover, the FOPID controller provides faster dynamic response, lower overshoot, and improved stability compared to the conventional PI controller.

Therefore, the proposed FOPID-controlled transformer-less solar micro-inverter system offers enhanced power quality, higher efficiency, superior transient performance, and improved grid compliance, making it a suitable solution for modern grid-connected photovoltaic applications.

TABLE III

COMPARSION TABLE

Parameters	**Existing System (PI Controller)**	**Extension System (FOPID Controller)**
PV Output Power	4.5 kW	4.9 kW
Grid Voltage	230 V	230 V
Grid Current	21 A	22 A
DC Link Voltage	600 V	600 V
Rise Time	0.45 sec	0.22 sec
Settling Time	0.80 sec	0.35 sec
Overshoot	12%	4%
Steady State Error	2.5%	0.6%
Grid Current THD	3.85%	1.17%

Grid Voltage THD	2.33%	0.69%
Power Factor	0.94	0.99
System Efficiency	91%	97%
Controller Response	Moderate	Fast
Stability	Normal	Improved

CONCLUSION

This work presented an advanced Fractional-Order Proportional–Integral–Derivative (FOPID) controlled transformer-less solar micro-inverter incorporating an effective power decoupling technique for single-phase grid-connected photovoltaic applications. The proposed topology successfully eliminates the requirement of a bulky line-frequency transformer, resulting in reduced size, weight, cost, and power losses while improving overall system efficiency. The integration of the FOPID controller significantly enhanced the dynamic performance of the micro-inverter by providing faster response, improved stability, superior tracking capability, and better adaptability under varying solar irradiance and grid conditions. Compared with the conventional PI controller, the proposed FOPID-based control strategy demonstrated improved transient characteristics, reduced overshoot, lower settling time, and minimized steady-state error. Furthermore, the grid current and voltage waveforms exhibited lower harmonic distortion, thereby enhancing power quality and ensuring compliance with grid interconnection standards. The implemented power decoupling mechanism effectively suppressed double-line frequency power oscillations, reducing the dependence on large electrolytic capacitors and consequently improving system reliability and operational lifetime. Simulation results verified the effectiveness of the proposed system, showing enhanced power extraction, improved power factor, reduced Total Harmonic Distortion (THD), and higher conversion efficiency. The common-ground transformer-less configuration also minimized leakage current, making the system suitable for practical residential and commercial grid-connected PV installations.

Future research can focus on the hardware implementation and experimental validation of the proposed micro-inverter under real-time operating conditions. Advanced optimization techniques such as Particle Swarm Optimization (PSO), Grey Wolf Optimization (GWO), and Artificial Intelligence (AI)-based tuning methods may be employed to further enhance the FOPID controller performance. Additionally, the integration of energy storage systems, smart grid communication capabilities, reactive power support, fault ride-through operation, and grid-support functionalities can be investigated to improve system flexibility and reliability. The proposed approach can also be extended to microgrid and hybrid renewable energy systems to facilitate efficient and sustainable energy management.

REFERENCES

[1] Ministry of New and Renewable Energy (MNRE), Government of India, "National Solar Mission," New Delhi, India, 2022.

[2] Q. Li and P. Wolfs, "A review of the single phase photovoltaic module integrated converter topologies with three different DC link configurations," IEEE Trans. Power Electron., vol. 23, no. 3, pp. 1320–1333, May 2008.

[3] S. B. Kjaer, J. K. Pedersen, and F. Blaabjerg, "A review of single-phase grid-connected inverters for photovoltaic modules," IEEE Trans. Ind. Appl., vol. 41, no. 5, pp. 1292–1306, Sept.–Oct. 2005.

[4] H. Xiao and S. Xie, "Transformerless split-inductor neutral point clamped three-level PV grid-connected inverter," IEEE Trans. Power Electron., vol. 27, no. 4, pp. 1799–1808, Apr. 2012.

[5] R. Gonzalez, J. Lopez, P. Sanchis, and L. Marroyo, "Transformerless inverter for single-phase photovoltaic systems," IEEE Trans. Power Electron., vol. 22, no. 2, pp. 693–697, Mar. 2007.

[6] T. Kerekes, R. Teodorescu, P. Rodriguez, G. Vazquez, and E. Aldabas, "A new high-efficiency single-phase transformerless PV inverter topology," IEEE Trans. Ind. Electron., vol. 58, no. 1, pp. 184–191, Jan. 2011.

[7] F. Blaabjerg, M. Liserre, and K. Ma, "Power electronics converters for wind turbine systems," IEEE Trans. Ind. Appl., vol. 48, no. 2, pp. 708–719, Mar.–Apr. 2012.

[8] Y. Sun, Y. Su, and X. Wang, "A high-efficiency transformerless photovoltaic micro-inverter with power decoupling capability," IEEE Trans. Power Electron., vol. 31, no. 7, pp. 4910–4921, Jul. 2016.

[9] S. Jain and V. Agarwal, "A single-stage grid connected inverter topology for solar PV systems with maximum power point tracking," IEEE Trans. Power Electron., vol. 22, no. 5, pp. 1928–1940, Sept. 2007.

[10] M. Islam, S. Mekhilef, and M. Hasan, "Single-phase transformerless inverter topologies for grid-tied photovoltaic systems: A review," Renewable Sustainable Energy Rev., vol. 45, pp. 69–86, May 2015.

[11] S. V. Araujo, P. Zacharias, and R. Mallwitz, "Highly efficient single-phase transformerless inverters for grid-connected photovoltaic systems," IEEE Trans. Ind. Electron., vol. 57, no. 9, pp. 3118–3128, Sept. 2010.

[12] I. Podlubny, "Fractional-order systems and PIλDμ controllers," IEEE Trans. Autom. Control, vol. 44, no. 1, pp. 208–214, Jan. 1999.

[13] C. A. Monje, Y. Chen, B. M. Vinagre, D. Xue, and V. Feliu, Fractional-Order Systems and Controls: Fundamentals and Applications. London, U.K.: Springer, 2010.

[14] D. Valério and J. S. da Costa, "An introduction to fractional control," IET Control Theory Appl., vol. 5, no. 8, pp. 1033–1057, May 2011.

[15] Y. Luo and Y. Chen, Fractional Order Motion Controls. Hoboken, NJ, USA: Wiley-IEEE Press, 2012.

[16] A. G. Radwan and K. N. Salama, "Fractional-order RC and RL circuits," Circuits Syst. Signal Process., vol. 31, no. 6, pp. 1901–1915, Dec. 2012.

[17] A. Lashab, D. Sera, J. M. Guerrero, and L. Mathe, "A fractional-order PID controller for grid-connected photovoltaic systems," IEEE Access, vol. 8, pp. 103596–103607, 2020.

[18] M. Liserre, F. Blaabjerg, and S. Hansen, "Design and control of an LCL-filter-based three-phase active rectifier," IEEE Trans. Ind. Appl., vol. 41, no. 5, pp. 1281–1291, Sept.–Oct. 2005.

[19] J. M. Guerrero, J. C. Vasquez, J. Matas, L. G. de Vicuña, and M. Castilla, "Hierarchical control of droop-controlled AC and DC microgrids," IEEE Trans. Ind. Electron., vol. 58, no. 1, pp. 158–172, Jan. 2011.

[20] F. Blaabjerg, Y. Yang, D. Yang, and X. Wang, "Distributed power-generation systems and protection," Proc. IEEE, vol. 105, no. 7, pp. 1311–1331, Jul. 2017.